RESEARCH PAPER

Preparation, Formulation, and Characterization of novel *Artemisia annua L.* Nanoemulsion for management of Diabetes

Mohd Masih Uzzaman Khan*, Faris Khalid AlForaiheedi
Department of Pharmaceutical Chemistry & Pharmacognosy, College of Pharmacy, Qassim University, Saudi Arabia

***Corresponding author:**
Email: Mo.khan@qu.edu.sa; 441109843@qu.edu.sa; Orcid ID; 0000-0002-2562-7403 (Dr. Mohd Masih Uzzaman Khan)

Abstract
This study reports the systematic development and optimization of a nanoemulsion-based delivery system for *Artemisia annua L.* to enhance its antidiabetic efficacy and bioavailability. The hydroalcoholic extract yielded a 12.8% w/w semisolid extract containing flavonoids, terpenoids, and tannins. A 2^3 full factorial design was applied to optimize the formulation variables (Tween 80, PEG 400, and Camelina sativa oil). Among the eight experimental batches, formulation F6 (24% Tween 80, 10% PEG 400, 7% oil) demonstrated optimal characteristics with a nanoscale particle size of 112.9 nm, high entrapment efficiency (89.2%), and zeta potential of –27.7 mV, indicating good colloidal stability. The optimized nanoemulsion exhibited a near-neutral pH (7.02 ± 0.04), suitable viscosity (78.45 ± 0.42 cP), and controlled drug release (98.78 ± 2.59% over 12 h) following Higuchi diffusion kinetics (R^2 = 0.9448). Stability studies confirmed the preservation of physicochemical parameters for 3 months under accelerated conditions. In a streptozotocin–nicotinamide-induced type 2 diabetic rat model, the nanoemulsion (200 mg/kg) produced significant antihyperglycemic effects (–126.1 mg/dL), improved body weight (+61.6 g), corrected dyslipidemia (notably TC –43.0 mg/dL and LDL –40.6 mg/dL), restored antioxidant defenses (CAT +15.1 U/mg; MDA –3.1 nmol/mL), and normalized hepatic biomarkers (SGPT –33.9 U/L), with efficacy comparable to metformin. These findings demonstrate that nanoemulsion-mediated delivery substantially enhances the therapeutic performance of the A. annua extract. This study provides a scalable nanotechnology-based strategy for improving phytopharmaceutical efficacy, offering globally relevant insights for the development of plant-derived interventions for type 2 diabetes management.
Keywords*: Artemisia annua; Nanoemulsion; Antioxidants; Antidiabetic activity; Factorial design; Oxidative stress; Lipid profile*

How to cite this article: Khan MMU, AlForaiheedi FK. Preparation, Formulation, and Characterization of Novel Artemisia annua L. Nanoemulsion for Management of Diabetes. Int J Drug Deliv Technol. 2026;16(35s): 1073-1090. DOI: 10.25258/ijddt.16.35s.120

Graphical Abstract:

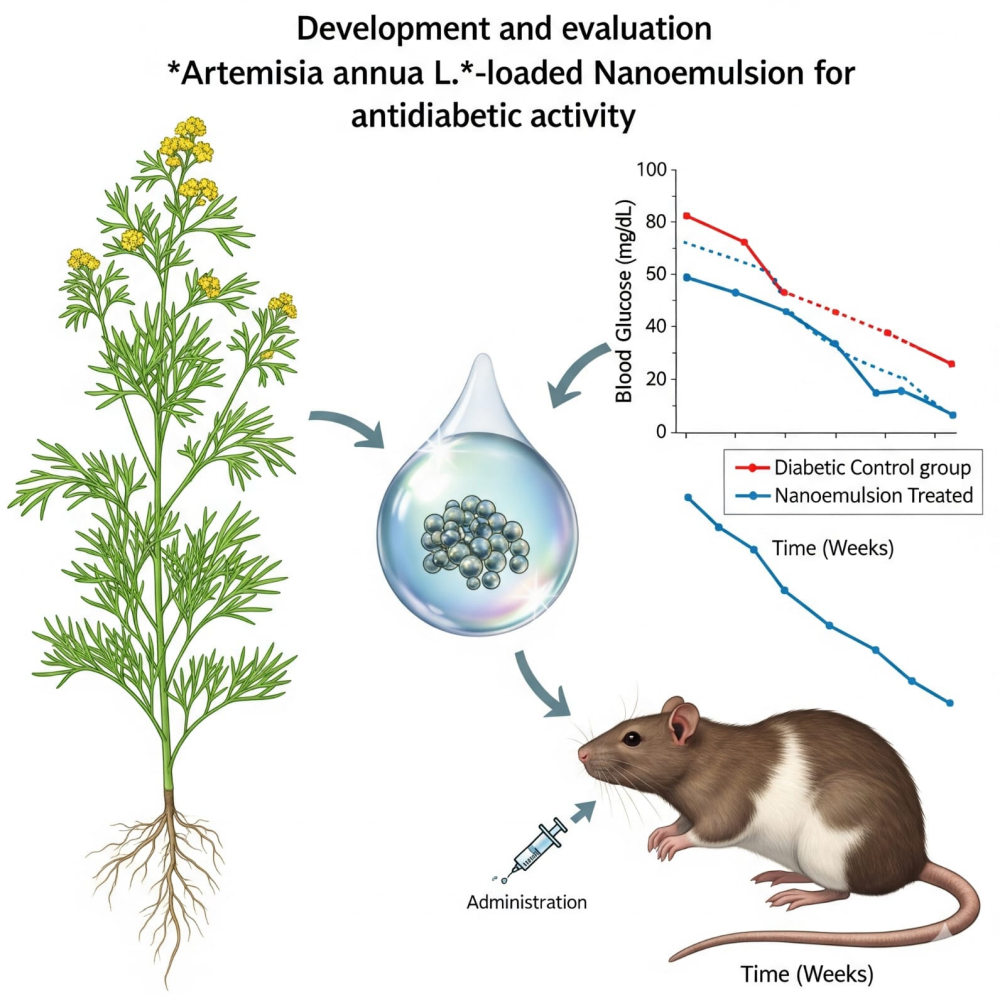

Introduction

Diabetes mellitus is a severe metabolic condition characterized by sustained hyperglycemia resulting from inadequate insulin production, resistance, or both. The prevalence of type 2 diabetes mellitus (T2DM) is increasing globally, with significant contributions to morbidity and mortality due to associated complications such as dyslipidemia, oxidative stress, and hepatic dysfunction [1–5]. Current pharmacological therapies, including metformin, sulfonylureas, and insulin, provide effective glycemic control but are often limited by side effects, reduced patient compliance, and inability to fully address the oxidative and inflammatory pathways contributing to disease progression. Consequently, there is a growing demand for plant-derived therapeutics with multi-target actions and improved safety profiles. Complementary and alternative medicine approaches, particularly phytotherapy, have gained considerable attention because they offer bioactive compounds capable of modulating multiple pathogenic mechanisms simultaneously, such as insulin resistance, pancreatic β-cell dysfunction, and inflammation.

In recent years, green nanotechnology and advanced functional materials have emerged as transformative tools for improving human health, while simultaneously addressing environmental and economic challenges. Eco-friendly synthetic strategies utilizing plant extracts, biodegradable polymers, and low-energy fabrication routes have been widely applied in environmental remediation, chemical sensing, energy storage systems, and biomedical applications. For example, green-synthesized nanostructured materials have demonstrated efficient electrochemical sensing performance for food safety monitoring, advanced nanoparticle fabrication via sustainable routes, eco-friendly nanomaterials for sensing and electronic applications, and green-fabricated nanocomposites for analytical measurement systems [6–9]. These studies highlight the versatility, scalability, and environmental compatibility of green nanomaterials across multiple fields. Such developments support the translation of sustainable nanotechnology into pharmaceutical and medical domains [10–13].

Artemisia annua L., a medicinal plant belonging to the Asteraceae family, has garnered significant attention for its many pharmacological characteristics, including antimalarial, antioxidant, anti-inflammatory, and antidiabetic effects [14–16]. Phytochemical investigations of Artemisia annua L. have identified flavonoids, terpenoids, tannins, saponins, and phenolic substances, which together contribute to glucose reduction, lipid modulation, and free radical scavenging activity. Several studies have suggested that these bioactive compounds may improve insulin sensitivity, reduce postprandial hyperglycemia, and protect pancreatic tissue from oxidative damage. However, the therapeutic use of Artemisia annua L. is limited by inadequate solubility, reduced bioavailability, and the instability of its bioactive constituents when taken orally in crude form, restricting its clinical utility despite its proven pharmacological potential [17–20].

To overcome these limitations, nanotechnology-based delivery systems fabricated using green and sustainable approaches are increasingly being explored. Nanoemulsions, polymer–bioactive composites, and plant-mediated nanostructures provide enhanced solubility, stability, and controlled release, while minimizing toxic residues and production costs. Green-fabricated nanostructures reported in recent sensor and materials research have demonstrated improved surface reactivity, nanoscale uniformity, and stability, which are directly translatable to pharmaceutical nanoformulations [6–8]. Thus, integrating sustainable nanomaterial design with phytotherapeutic development represents an innovative strategy to enhance therapeutic performance while aligning with the global sustainability goals.

Nanotechnology-driven drug delivery systems, especially nanoemulsions, have arisen as effective methods to improve the solubility, stability, and absorption of weakly water-soluble plant constituents [21,22]. Nanoemulsions are kinetically stable colloidal dispersions consisting of oil, surfactants, and water, with droplet sizes often between 20 and 200 nm. Their high surface area and thermodynamic stability facilitate enhanced absorption and controlled release, improving pharmacological efficacy at lower doses. Additionally, nanoemulsions can protect labile bioactive compounds from enzymatic degradation and gastrointestinal metabolism. Moreover, the incorporation of natural stabilizers, such as pectin, offers additional benefits by imparting stability, mucoadhesion, and biocompatibility, further enhancing bioavailability [10–13]. Such delivery systems are increasingly being recognized for their potential to optimize the therapeutic performance of herbal extracts while minimizing systemic toxicity.

Despite significant progress in green nanomaterials for environmental, sensing, and energy-related applications, few studies have comprehensively translated these sustainable fabrication principles into optimized nanoformulations for antidiabetic phytomedicine. Therefore, developing an Artemisia annua L.-based nanoemulsion through systematic design and sustainable formulation principles addresses both therapeutic and environmental innovation gaps.

In this study, we developed and optimized an Artemisia annua L.–loaded nanoemulsion using a 2^3 factorial design. Tween 80, PEG 400, and Camelina sativa oil were selected as critical formulation variables to systematically assess their effects on particle size and entrapment efficiency. The improved composition was evaluated using droplet size analysis, zeta potential (ZP) measurements, viscosity assessment, pH determination, surface morphology examination, drug release kinetics, and stability testing under accelerated procedures.

Therapeutic potential was assessed by comparing the optimized nanoemulsion with crude Artemisia annua L. extract in streptozotocin-nicotinamide-induced hyperglycemic Wistar rats. Antidiabetic effectiveness was evaluated based on body weight, fasting blood glucose, lipid profile, oxidative stress biomarkers, and hepatic enzyme indicators. The quantitative results were statistically analyzed to determine the relative efficacy of the nanoemulsion versus the extract. By integrating green nanotechnology concepts with phytopharmaceutical optimization, this study contributes to sustainable nanomedicine development and provides a globally relevant platform for improving plant-based therapies for metabolic disorders.

Material and Method

Materials

Polyethylene glycol 400 (PEG 400), Tween 80, Camelina sativa oil, and pectin were used as the excipients. All chemicals and solvents were of analytical grade and used without further purification.

Methods

Collection and Extraction of Plant Material

Artemisia annua L. powder was purchased from Agro-Food Processing Emporium. Approximately 50 g of powder was mixed with 500 mL of 70% ethanol (1:10 w/v) and subjected to ultrasonic-assisted extraction using an ultrasonic probe (20 kHz, 750 W) operated at 50% amplitude in pulsed mode for 30 min while

maintaining the temperature at 30–35 °C. The extract was filtered and the residue was re-extracted under identical conditions. filtrates were combined and concentrated under reduced pressure at 40–45 °C using a rotary evaporator to remove solvent. The resulting extract was dried to semisolid consistency, weighed, and stored at 4 °C in amber glass vials until use.

Qualitative Phytochemical Screening

The crude hydroalcoholic extract of *Artemisia annua L.* was evaluated for the presence of major phytoconstituents using standard phytochemical tests. Alkaloids were identified using Dragendorff's and Mayer's reagents, flavonoids using the Shinoda test, saponins using the frothing test, tannins and phenolics using ferric chloride solution, terpenoids using Salkowski's test, and glycosides using the Keller–Killiani reaction. Preliminary screening identified the presence of many bioactive compounds, such as alkaloids, flavonoids, terpenoids, tannins, and saponins, all of which are known for their pharmacological effects, including antidiabetic and anti-inflammatory activity [14,23–26].

Preparation of Standard Calibration Curve of the Extract in Ethanol

A stock solution was prepared by dissolving 100 mg of *Artemisia annua L.* extract in 5 ml of ethanol and adjusting the volume to 100 ml using the same solvent. Various dilutions were prepared from this sample to achieve concentrations between 10 µg/mL and 80 µg/ml. The solutions were examined using a UV spectrophotometer to determine their maximum absorbance wavelength (λmax). The absorbance of each diluted sample was measured at λmax, and a calibration curve was constructed with the concentration (µg/ml) on the X-axis and absorbance on the Y-axis. The linearity of the plot was validated according to Beer's law. The calibration graph was then used to ascertain the concentration of the medication released during the in vitro dissolution tests [27,28].

Determination of Extract–Polymer Compatibility

FTIR spectra of *Artemisia annua L.* extract and excipients had been obtained using KBr pellet method over 4000–400 cm^{-1}. DSC thermograms of the extract, excipients, and their blends had been recorded in the range of 30–350 °C under nitrogen purge [29–33].

Preparation of *Artemisia Annua L* loaded Nanoemulsion

Based on visual observations, such as transparency and ZP, eight formulations were selected according to the 2^3 factorial design (Table 1) for the preparation of *Artemisia annua L.*-loaded pectin-stabilized nanoemulsions. The formulations were prepared using a high-energy emulsification technique by varying the concentrations of Tween 80 (surfactant), PEG 400 (co-surfactant), and Camelina sativa oil (oil phase) at two levels. The aqueous phase was prepared by dissolving pectin and methyl paraben in purified water and preheating the mixture at 40–50°C. Separately, Camelina sativa oil was slowly incorporated into Smix (Tween 80/PEG 400) under continuous stirring, followed by gradual addition of the pectin-containing aqueous phase to obtain coarse emulsions. These coarse emulsions were further processed by high-pressure homogenization at 15,000 psi for 5–7 cycles, producing nanosized droplets within the range of 20–200 nm. Pectin served as a natural stabilizer, providing interfacial protection and viscosity enhancement, thereby improving droplet stability. Finally, the nanoemulsions were cooled to room temperature and stored in amber vials for subsequent evaluation [34–36].

Factorial Design

Design and optimization of formula with *Artemisia annua L.*

A 2^3 full factorial design was employed using Design-Expert® software to optimize the nanoemulsion formulation containing *Artemisia annua L.* Three independent variables, surfactant concentration (X1=18-24%), co-surfactant concentration (X2=6-10%), and oil concentration (X3=5-7%), were selected based on their potential impact on the formulation's characteristics. The dependent variables used to evaluate the performance were particle size (Y1) and entrapment efficiency (Y2). Eight formulations were generated to cover all combinations of the selected factor levels, and each formulation was evaluated for the defined responses. The experimental data were statistically analyzed using ANOVA and model fitting to determine the optimal conditions for achieving minimal particle size and maximum entrapment efficiency. The factorial design batches are listed in Tables 1 and 2, respectively.

Table 1. Levels of variables for optimization

Sr. No.	Factor	Low level (%)	High Level (%)
1	Surfactant (Tween 80)	18	24
2	Co-surfactant (PEG 400)	06	10
3	Oil (Camelina sativa oil)	05	07

Table 2. Factor level for 2^3 Full Factorial Designs

Batch Code	X1: Surfactant (%)	X2: Co-surfactant (%)	X3: Oil (%)
F1	24	6	7
F2	18	10	5
F3	24	6	5
F4	18	10	7
F5	18	6	7
F6	24	10	7
F7	18	6	5
F8	24	10	5

Properties of Nano-emulsion

Physical properties

The prepared nano-emulsion formulations were carefully inspected visually to assess their color, clarity, overall uniformity, and physical consistency to ensure the quality and stability of the system.

Size Distribution and Size of Droplet

Droplet size was measured using PCS with a Zetasizer (Malvern 1000 HS) by analyzing light scattering of nanoemulsion (0.1 ml in 50 ml water) at 25°C and 90° angle.

Zeta potential (ZP)

ZP refers to the overall net electrical charge carried by the surface of droplets dispersed in a particular medium. Understanding and measuring the ZP of a nanoemulsion is essential, as it provides valuable information about the electrostatic repulsion between particles, and thereby helps in evaluating the physical stability and shelf-life of the formulation during storage.

Viscosity determination

viscosity of Nanoemulsion was measured using a Brookfield viscometer with using spindle number 62 at 25°C. A sample volume of 30 ml was used and was subjected to various rpm, for example, 5, 10, 20, 50, and 100, and the rheological behavior of the disperse system was examined by constructing a theological gram of shear stress vs. shear stress rate.

Measurement of pH

Nanoemulsion pH was measured at 25°C using a calibrated digital pH meter (with pH 4 and 7 buffers) on a 10% w/w dispersion (1 g in 10 ml distilled water).

SEM

The surface morphology of the prepared nanoemulsion was examined using scanning electron microscopy (SEM, Carl Zeiss SEM equipped with Oxford EDX). For the analysis, a small quantity of the nanoemulsion was carefully placed onto Formvar-coated copper grids, excess liquid was removed, and the sample was allowed to dry before imaging.

***In-vitro* Release Study**

In-vitro permeation studies were performed using a Franz diffusion cell fitted with a dialysis membrane, where the receptor compartment contained 25 ml of phosphate buffer (pH 7.4). The entire setup was positioned on a magnetic stirrer and continuous agitation of the receptor medium was maintained with magnetic beads at a speed of 100 rpm. The temperature of the system was carefully regulated and maintained at 37 ± 0.5 °C for the duration of the experiment to simulate physiological conditions. The amount of oil permeated was quantitatively estimated using a UV–Visible spectrophotometer at a detection wavelength of 272 nm.

Kinetics of Drug Release

The in vitro drug release data were fitted to various kinetic models to determine the drug release mechanism. Zero-order kinetics were assessed by plotting cumulative drug release versus time, whereas first-order kinetics used the logarithm of the remaining drug percentage against time. The Higuchi model examines diffusion-controlled release by plotting cumulative release against the square root of time. The Korsmeyer–Peppas model involved plotting the logarithm of cumulative release versus the logarithm of time to calculate the release exponent (n) and further characterize the mechanism.

Stability Study

stability of the optimized nanoemulsion was tested per ICH guidelines for 3 months at 40±5°C and 70±5% RH in amber glass bottles. After three months, the nano-emulsion was tested for pH, ZP, and viscosity.

***In vivo* Antidiabetic Activity of Extract and Optimized Nanoemulsion**

Chemicals and Reagents

The drugs used were *Artemisia annua* extract (AAE) and *Artemisia annua* Nanoemulsion (AAN). All reagents and chemicals employed in this study were of analytical grade. Streptozotocin (STZ), nicotinamide, and metformin hydrochloride were purchased from Sigma-Aldrich (USA). Diagnostic assay kits for blood glucose, lipid profile, hepatic enzymes, and antioxidant markers were obtained from Span Diagnostics (India) and Thermo Fisher Scientific (USA), respectively. STZ solutions were freshly prepared prior to administration in cold 50 mM citrate buffer (pH 4.5) to preserve their stability.

Experimental Animals

Adult male Wistar albino rats, weighing between 180 and 250 g, were procured from an institutional animal breeding facility for use in this study. The animals were maintained in clean polypropylene cages under well-regulated laboratory conditions, including a controlled

temperature of 25 ± 2°C, relative humidity of approximately 55%, and a standard 12-hour light/dark cycle. They were provided free access to a balanced pellet diet and drinking water throughout the experimental period. The study protocol was approved by the Institutional Animal Ethics Committee (IAEC) following the guidelines prescribed by the Committee for the Purpose of Control and Supervision of Experiments on Animals (CPCSEA) (Approval No. 10/IAEC-II/SLSRPL/2025).

Acute Oral Toxicity Evaluation

An acute oral toxicity study of AAE was performed in female Wistar rats (n = 6) following OECD Guideline 423. Rats were fasted overnight, received a single oral dose of 2000 mg/kg, observed for 24 h for immediate toxicity, and monitored for 14 days for clinical signs, body weight, food and water intake, and general health. At the end of the study, necropsy of the major organs (liver, kidneys, heart, lungs, and spleen) revealed no pathological changes or mortality, indicating a wide safety margin. Based on these results, therapeutic doses of 100 and 200 mg/kg were selected for efficacy studies.

Induction of Experimental T2DM

T2DM was induced in the rats after overnight fasting. A single intraperitoneal injection of nicotinamide at a dosage of 120 mg/kg body weight was administered, followed 15 min later by streptozotocin (65 mg/kg body weight) freshly dissolved in cold citrate buffer (pH 4.5). To avert acute hypoglycemia post-induction, the animals were administered a 10% sucrose solution for the first 24 h. Seventy-two hours after induction, fasting blood glucose levels were assessed using a glucometer, and animals exhibiting glucose concentrations of ≥ 200 mg/dL were designated as diabetic and chosen for further experimental treatments.

Experimental Design and Treatment Protocol

Following successful induction of diabetes, the animals were randomly allocated into five experimental groups (n = 6 per group) (Table 3), as outlined below:

Table 3. Experimental groups and treatment regimen

Group	*Description*	*Induction*	*Treatment Administered*
I	Normal Control	No	1% gum acacia (vehicle)
II	Diabetic Control	STZ + Nicotinamide	1% gum acacia (vehicle)
III	Standard Drug Group	STZ + Nicotinamide	Metformin 100 mg/kg
IV	AAE (Low Dose)	STZ + Nicotinamide	100 mg/kg b.w.
V	AAE (High Dose)	STZ + Nicotinamide	200 mg/kg b.w.
VI	AAN	STZ + Nicotinamide	200 mg/kg b.w.

All therapies were administered orally once daily by oral gavage for 21 consecutive days. Fasting blood glucose levels and body weight were assessed on days 0, 7, 14, and 21 of the treatment intervals.

Biochemical and Oxidative Stress Evaluation

At the end of the study, the animals were fasted overnight and anesthetized for blood collection via the retro-orbital plexus. Serum was separated by centrifugation and analyzed for biochemical and oxidative stress markers. Lipid profile parameters included total cholesterol (TC), triglycerides (TG), HDL-C, LDL-C, and VLDL-C, while liver function was assessed using SGOT/AST and SGPT/ALT levels. Antioxidant and oxidative stress status were evaluated by measuring the levels of superoxide dismutase (SOD), catalase, malondialdehyde (MDA), and reduced glutathione (GSH). All analyses were performed using standard spectrophotometric methods, following the validated manufacturer's protocols.

Statistical Analysis

All data are presented as mean ± standard error of the mean for each experimental group, with a sample size of six (n = 6). Statistical comparisons between groups were conducted using one-way ANOVA, followed by Tukey's post hoc multiple comparison test to evaluate inter-group differences. Differences were considered statistically significant at a p-value of less than 0.05.

Results and Discussion

Physical Characterization and Evaluation of Extract

Hydroalcoholic extraction yielded a 12.8% w/w semisolid extract, indicating the effective recovery of phytoconstituents using ultrasonic-assisted extraction. The moderate yield reflects the efficient extraction of both polar and moderately nonpolar compounds, consistent with the solvent system employed. Ultrasonication likely enhances solvent penetration and cellular disruption, facilitating improved mass transfer. The brownish-green appearance further supported the presence of chlorophyll derivatives,

flavonoids, and phenolic compounds, which are widely associated with antioxidant and antidiabetic activities.

Qualitative Phytochemical Analysis

Phytochemical screening confirmed the presence of flavonoids, phenolics, terpenoids, alkaloids, tannins, saponins and glycosides (Table 4). Collectively, these bioactive classes justify the therapeutic relevance of Artemisia annua. Flavonoids and phenolic compounds contribute to antioxidant activity and enzyme inhibition (α-amylase/α-glucosidase), whereas terpenoids may enhance insulin sensitivity. The detection of multiple secondary metabolites supports a multi-target pharmacological mechanism, which is advantageous for managing multifactorial disorders such as T2DM. The absence of steroids reduces concerns regarding the steroid-associated metabolic effects.

Table 4. Qualitative phytochemical screening of *Artemisia annua L.* hydroalcoholic extract

Phytochemical Class	Test Performed	Observation	Result
Alkaloids	Mayer's, Dragendorff's	Orange-red precipitate, cream ppt	++
Flavonoids	Shinoda, Alkaline reagent	Pink to red coloration, yellow color	++
Tannins	Ferric chloride, Lead acetate	Blue-black coloration, white ppt	+
Saponins	Froth test	Stable persistent froth	++
Glycosides	Keller–Killiani	Brown ring at interface	+
Terpenoids	Salkowski	Reddish-brown layer	+
Steroids	Liebermann–Burchard	No color change	–
Phenolic compounds	Ferric chloride	Bluish-green coloration	++
Carbohydrates	Molisch's	Violet ring at interface	+
Proteins & amino acids	Biuret, Ninhydrin	No violet/purple coloration	–

These phytoconstituents may contribute to the antidiabetic potential of the extract. Flavonoids and phenolic compounds are known to inhibit α-amylase and α-glucosidase, thereby reducing postprandial glucose levels and exerting antioxidant effects that protect the pancreatic β-cells from oxidative stress. Terpenoids may enhance insulin sensitivity and peripheral glucose utilization, whereas alkaloids, tannins, and saponins are associated with modulation of glucose metabolism and delayed carbohydrate absorption. The combined presence of these bioactive compounds supports the therapeutic relevance of this extract in diabetes management.

UV Spectroscopy

The UV–Visible spectral analysis of *Artemisia annua* L. extract was performed over a scanning range of 200–400 nm to identify its characteristic absorption maxima. The spectrum exhibits a prominent absorption peak at 275 nm (Figure 1), which is typically associated with the π→π* electronic transitions of aromatic rings and conjugated systems present in phenolic and flavonoid compounds. The presence of this well-defined λmax confirmed the abundance of chromophoric phytoconstituents in the extracts.

The detection of a single sharp absorption maximum also indicates minimal spectral interference and supports the suitability of 275 nm as the analytical wavelength for subsequent quantitative estimation during calibration and in vitro release studies. The observed λmax is consistent with previously reported spectral characteristics of *Artemisia annua*, thereby validating the identity and stability of the extract used in formulation development.

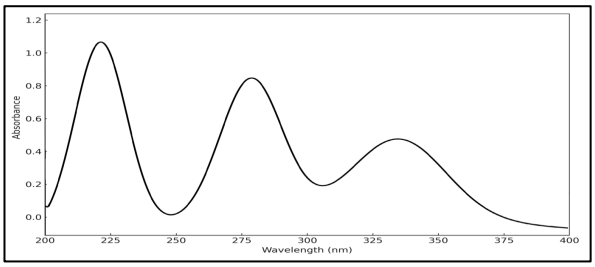

Figure 1. UV spectrum of *Artemisia Annua* L

Standard calibration curve

A standard calibration curve of the *A. annua L.* extract was constructed over a concentration range of 10–80 µg/mL to validate the analytical method for quantitative estimation. The absorbance values increased proportionally with concentration, demonstrating a clear linear relationship within the selected range, and confirming adherence to Beer–Lambert's law.

As shown in Table 5, the mean absorbance values progressively increased from 0.121 ± 0.02 at 10 µg/mL

to 0.828 ± 0.03 at 80 µg/mL. The relatively low standard deviation at each concentration level indicated good precision and minimal instrumental variability. The near-uniform increase in absorbance between successive concentrations confirms the sensitivity and reliability of the method across the working range.

The linear profile illustrated in Figure 2 further supports the robustness of the calibration model and validates its suitability for the accurate quantification of extract concentration during in vitro release and formulation analysis. Overall, the calibration data confirm that the developed spectrophotometric method is precise, reproducible, and appropriate for the analytical applications in this study.

Table 5. Standard calibration curve of *Artemisia Annua* L in Ethanol

Sr. No	Concentration (µg/ml)	Mean Absorbance (n=3; ± SD)
1	0	0
2	10	0.121±0.02
3	20	0.241±0.04
4	40	0.474±0.06
5	60	0.697±0.06
6	80	0.828±0.03

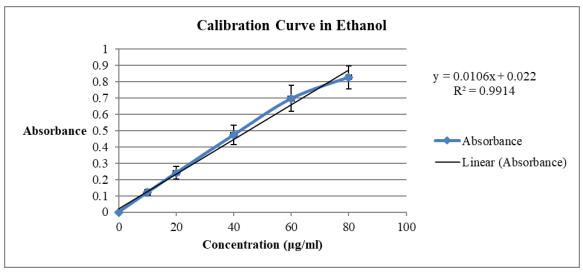

Figure 2. Standard calibration curve of *Artemisia Annua* L in Ethanol

Determination of drug-polymer compatibility

FTIR Spectroscopy

The FTIR spectra (Figure 3) of *Artemisia annua L.* extract, PEG-400, Tween-80, Camelina sativa oil, pectin, and their physical mixture were analyzed to assess the functional groups and compatibility. *Artemisia annua L.* exhibited a broad band around 3400 cm^{-1} corresponding to O–H stretching of phenolic and alcoholic groups, peaks at 2920–2850 cm^{-1} due to aliphatic C–H stretching, a sharp band near 1730 cm^{-1} attributed to carbonyl stretching of terpenoids and flavonoids, and characteristic C=C aromatic stretching around 1600–1500 cm^{-1}, along with C–O–C vibrations in the fingerprint region (1200–1000 cm^{-1}). PEG-400 showed a broad O–H band at 3400 cm^{-1}, C–H stretching bands at 2880–2860 cm^{-1}, and strong C–O–C stretching near 1100 cm^{-1}. Tween-80 displayed O–H stretching, C–H stretching, a strong ester carbonyl band at 1735 cm^{-1}, and ether linkages around 1100 cm^{-1}.

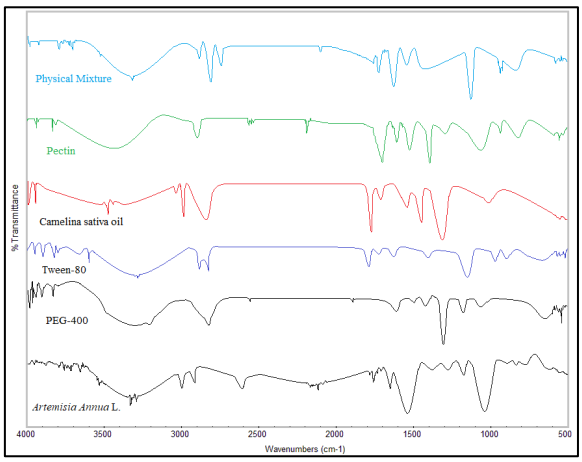

Figure 3. FTIR spectra of Extracts, Excipients and Physical Mixture

Camelina sativa oil showed prominent C–H stretching at 2925 and 2855 cm^{-1}, a sharp ester carbonyl band at 1740 cm^{-1}, CH_2/CH_3 bending peaks at 1460–1370 cm^{-1}, and C–O stretching vibrations at 1160–1090 cm^{-1}, confirming triglyceride structure. Pectin exhibited a broad O–H band near 3400 cm^{-1}, C–H stretching at 2920 cm^{-1}, a strong esterified carbonyl band at 1730 cm^{-1}, COO^- asymmetric stretching at 1600 cm^{-1}, and glycosidic C–O–C peaks between 1015 and 1050 cm^{-1}. The physical mixture retained all characteristic peaks of the individual components without significant shifts or disappearance, indicating the absence of chemical interactions and confirming the compatibility between *Artemisia annua* extract and the selected excipients.

Differential Scanning Calorimetry

The DSC thermograms (Figure 4) of *Artemisia annua L.* extract, PEG-400, Tween-80, Camelina sativa oil, pectin, and their physical mixture showed distinct, component-specific endothermic events and no appearance of new thermal events, indicating physical compatibility. The extract exhibited a sharp endotherm at 98.5°C (likely loss of adsorbed water and/or melting/softening of low-molecular-weight phytoconstituents), which is retained in the physical mixture with a minor up-shift to 99.1°C, suggesting only weak physical interactions (e.g., hydrogen bonding or miscibility) rather than chemical reactions.

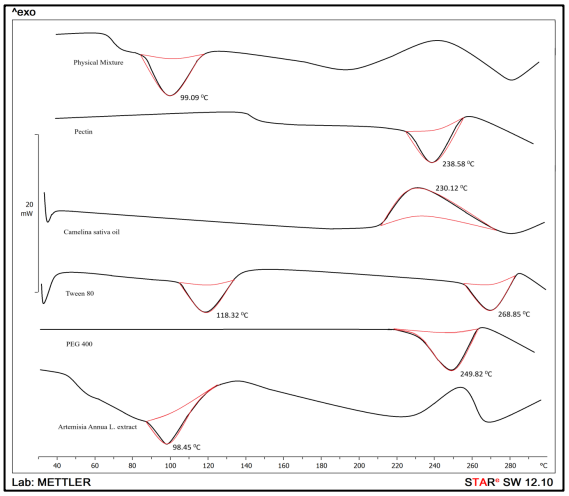

Figure 4. DSC graph of Extracts, Excipients and Physical Mixture

Tween-80 shows an endotherm near 118°C and a higher thermal event at 268–269°C. PEG-400 displays a major thermal transition at 250°C, Camelina sativa oil presents a broad endotherm centered 230°C (consistent with triglyceride melting/thermal rearrangement), and pectin exhibits an endotherm near 238–239°C attributable to depolymerization/thermal decomposition of the polysaccharide. In the physical mixture, the higher-temperature events were retained with slight broadening, confirming the thermal stability of the components and the absence of chemical incompatibility or new compound formation.

Preparation of *Artemisia Annua* L loaded Nanoemulsion

Based on visual observations, such as transparency and ZP, eight formulations were selected according to the 2^3 factorial design (Table 6) for the preparation of Artemisia Annua L-loaded nanoemulsions.

Formulation Design

Table 6. Factor level for 2^3 Full Factorial Designs

Batch Code	X1: Surfactant (%)	X2: Co-surfactant (%)	X3: oil (%)	Y1: Particle (nm)	Y2: %EE (%)
F1	24	6	7	119.6	85.7
F2	18	10	5	153.4	71.9
F3	24	6	5	131.8	79.6
F4	18	10	7	141.2	77.8
F5	18	6	7	146.5	75.4
F6	**24**	**10**	**7**	**112.9**	**89.2**
F7	18	6	5	158.1	69.7
F8	24	10	5	126.7	83.5

Table 6 presents the two factors at the lower, middle, and upper levels for both the coded and actual values. Responses Y1 and Y2 ranged from 112.9–158.1 d.nm and 69.7–89.2%, respectively. All responses from the nine prepared formulations were best described by the main effects model, as determined using Design Expert® software. The R^2, SD, and %CV values along with the regression equations for each response are provided in Tables 7 and 9. The ANOVA results (Tables 8 and 9) confirmed the significance of the model for all dependent variables. Independent variables X1, X2, and X3 positively influenced %EE, resulting in the desired nano-emulsion particle size.

Table 7. Summary of results of regression analysis for responses Y1 and Y2

Response Models Main Effect	R^2	Adjusted R^2	Predicted R^2	SD	%CV
(Y1)	0.9991	0.9983	0.9962	0.6595	0.4840
(Y2)	0.9968	0.9944	0.9871	0.5087	0.6431

Regression Equations

$Y1 = +136.38 - 13.52*A - 2.73*B + 6.23*C$ ---------- (9)

$Y2 = +79.10 + 5.40*A + 1.50*B - 2.92*C$ ---------- (10)

Model Assessment

The experimental data were analyzed using Design-Expert® software to evaluate the suitability of the statistical model for predicting the formulation responses. The Fit Summary analysis identified the Main Effect Model as the most appropriate for both particle size (Y1) and entrapment efficiency (%EE, Y2). The ANOVA results presented in Tables 8 and 9 confirm the statistical significance of the developed models, with p-values < 0.0001 for both responses, indicating a strong model reliability and predictive capability.

For particle size (Table 8), the model F-value (1404.46) and extremely low p-value (< 0.0001) demonstrated that the model terms were highly significant. Among the independent variables, surfactant concentration (A) exerted the most pronounced influence (F = 3364.15), followed by oil concentration (C), and co-surfactant (B). The very low residual sum of squares (1.74) indicated minimal unexplained variation, confirming a good model fit and low experimental error.

Similarly, for entrapment efficiency (Table 9), the model was highly significant ($F = 411.88$, $p < 0.0001$). The surfactant concentration again showed the

strongest effect (F = 901.57), highlighting its critical role in improving drug incorporation within nanoemulsion droplets. Oil concentration also significantly influenced %EE (F = 264.52), while the co-surfactant contributed moderately but significantly (p = 0.0011). The low residual value further confirms the adequacy of the model.

The regression equations indicate that variations in formulation variables directly impact the response magnitude, with surfactant concentration being the dominant factor affecting both droplet size reduction and entrapment enhancement. Overall, statistical analysis confirmed that the factorial design approach effectively optimized the formulation and reliably predicted the influence of critical process parameters on nanoemulsion performance.

Table 8. Results of Analysis of Variance for Measured Response (Particle Size)

Source	Sum of Squares	df	Mean Square	F-value	p-value	
Model	1832.81	3	610.94	1404.46	< 0.0001	**Significant**
A-Surfactant	1463.40	1	1463.40	3364.15	< 0.0001	
B-Co-Surfactant	59.40	1	59.40	136.56	0.0003	
C-Oil	310.01	1	310.01	712.66	< 0.0001	
Residual	1.74	4	0.4350			
Cor Total	1834.55	7				

Table 9. Results of Analysis of Variance for Measured Response (%EE)

Source	Sum of Squares	df	Mean Square	F-value	p-value	
Model	319.72	3	106.57	411.88	< 0.0001	**Significant**
A-Surfactant	233.28	1	233.28	901.57	< 0.0001	
B-Co-Surfactant	18.00	1	18.00	69.57	0.0011	
C-Oil	68.44	1	68.44	264.52	< 0.0001	
Residual	1.04	4	0.2588			
Cor Total	320.76	7				

Response Surface Plot Analysis

Particle size is a critical determinant of PNs and affects both the release and absorption of the extract. Smaller particles provide an increased surface area, thereby improving extract absorption and bioavailability. The polydispersity index (PDI), derived from the mean particle size, solvent refractive index, measurement angle, and distribution variance, signifies population uniformity; a low PDI denotes strong homogeneity, while a high PDI shows diverse or numerous size distributions. The 3D response surface map (Figure 5A) indicated that the nanoemulsion batch with the smallest particle size was the recommended optimal formulation. The investigation demonstrated that an elevated oil content (X3 = 7%) resulted in an enlarged particle size (F7:158.1 nm), whereas an adequate surfactant concentration (F6) preserved a smaller size (112.9 nm), underscoring the critical function of the surfactant in regulating droplet dimensions.

From the 3D response surface plot (Figure 5 B), In terms of entrapment efficiency (Y2), the 3D plot indicates that the prepared nanoemulsions exhibited entrapment efficiency values between 69.7% and 89.2%. The results revealed that increasing the surfactant (Tween 80) and co-surfactant (PEG 400) concentrations significantly reduced droplet size while improving entrapment efficiency. This can be attributed to the enhanced interfacial stabilization and increased solubilization of the Artemisia annua extract. Among the tested formulations, Batch F6 (24% Tween 80, 10% PEG 400, 7% Artemisia) showed the lowest particle size (112.9 nm) and highest %EE (89.2%), thereby representing the optimized formulation suitable for further evaluation.

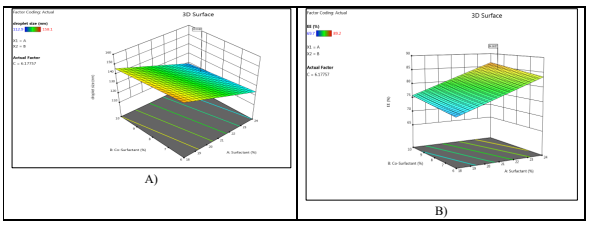

Figure 5. Response surface plots for X1, X2 and X3 on A) Mean Particle Size (Y1) and B) %EE (Y2)

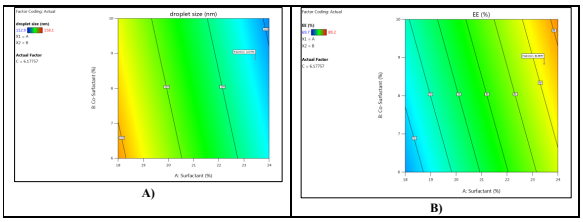

Figure 6. Contour plots for X1, X2 and X3 on A) Mean Particle Size (Y1) and B) %EE (Y2).

Figure 6 illustrates that the contour plots in QbD are graphical representations that depict the relationship between CQAs and CPPs. These plots are useful for visualizing the design space and understanding how changes in the process parameters may affect product quality. Both indicate a flat contour and that the critical quality attribute is relatively insensitive to changes in the associated process parameters within that region. This suggests a robust design space in which variations in these parameters are less likely to affect product quality. Both responses showed optimized results in the design space.

Characterization of Nanoemulsion

Physical Characterization

The nanoemulsions were visually inspected for color, clarity, uniformity, and consistency. All nanoemulsion batches (F1-F8) exhibited a consistent physical appearance characterized by a transparent, slightly white coloration. None of the formulations showed any signs of phase separation, which indicated good physical stability. However, all batches were heterogeneous, as shown in Figure 7.

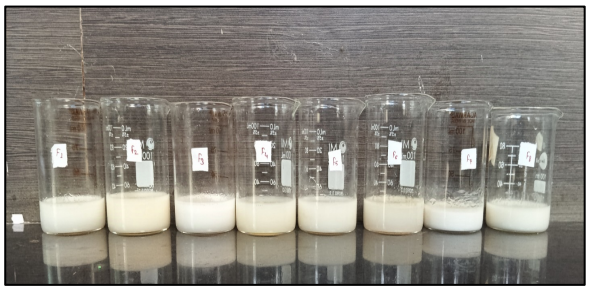

Figure 7. Physical Characterization

Droplet Size and Size Distribution

Particle size in nanoemulsions (NEs) is crucial, as it influences drug release and absorption; smaller particles provide a larger surface area, enhancing bioavailability. The polydispersity index (PDI), which includes the mean size, solvent refractive index, measurement angle, and distribution variance, reflects particle uniformity; low PDI indicates high homogeneity, while a high PDI suggests a wider size range. The optimized formulation (F6) exhibited a mean particle size of 112.9 nm with PDI of 0.534, as shown in Figure 8.

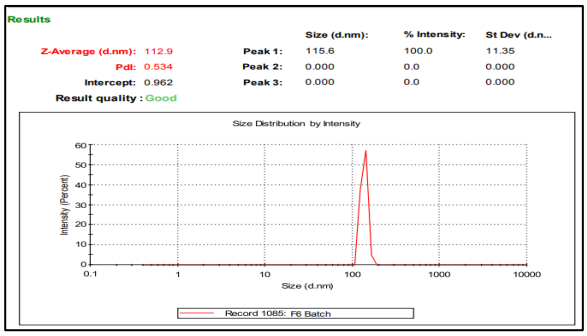

Figure 8. Particle size of F6 formulation

ZP

The ZP of the optimized drug-loaded nanoemulsion (F6) was found to be –27.7 mV (Figure 9). This value indicates adequate electrostatic repulsion between the dispersed droplets, which helps to prevent aggregation and coalescence during storage. In colloidal systems, ZP values approaching ±30 mV are generally considered indicative of good physical stability; therefore, the observed negative surface charge suggests a stable nanoemulsion system.

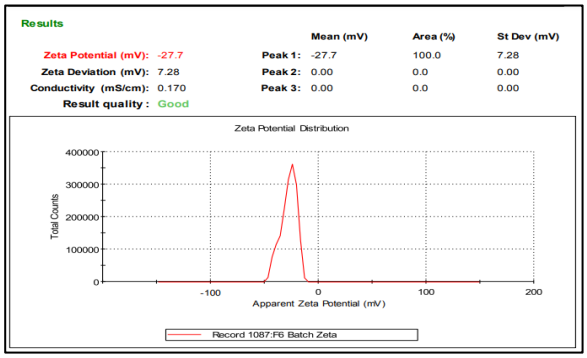

Figure 9. ZP of F6 formulation

Viscosity determination

The viscosity (Table 10) of the optimized nanoemulsion batch (F6) was evaluated using a Brookfield viscometer at varying spindle speeds to assess its rheological behavior. The results demonstrated shear-thinning behavior, where viscosity decreased with increasing shear rate, indicating non-Newtonian flow characteristics. At 10 RPM, the viscosity was highest at 78.45 ± 0.42 cP with a torque of 22.10%, which progressively decreased to 64.15 ± 0.33 cP at 50 RPM with a torque of 30.95%. Among all formulations, F6 exhibited the highest viscosity, suggesting better structural integrity and stability under low-shear conditions.

Table 10. Viscosity of Optimized batch of Nanoemulsion (F6)

Speed (RPM)	Viscosity(cP)	Torque (%)
10	78.45±0.42	22.10

20	75.63±0.35	39.85
30	71.92±0.29	37.40
40	69.48±0.41	34.22
50	64.15±0.33	30.95

Measurement of pH

The pH values of the nanoemulsion formulations F1 to F8 were found to range between 6.18±0.02 and 7.02±0.04, as presented in Table 11. These values fall within the normal pH range of the human skin (5–7), indicating that the formulations are unlikely to cause skin irritation. Among all formulations, F6 exhibited the highest pH (7.02 ± 0.04), while F5 had the lowest (6.18±0.02). Overall, the pH values confirmed that all the prepared nanoemulsion formulations were dermatologically suitable and safe for topical application.

Table 11. Characterization of Nanoemulsion

Formulation code	pH value
F1	6.88±0.03
F2	6.61±0.02
F3	6.90±0.01
F4	6.49±0.03
F5	6.18±0.02
F6	7.02±0.04
F7	6.52±0.02
F8	6.60±0.03

Surface Morphological Study

The surface morphology of the optimized nanoemulsion formulation (F6) was analyzed using SEM, as shown in Figure 10. The image reveals that the droplets were uniformly spherical in shape with smooth surfaces, indicating a well-formed and stable nanoemulsion structure. The observed particle sizes in the image range from 50.8 nm to 159.7 nm, closely aligning with the average droplet size of approximately 200 nm. However, based on dynamic light scattering or other size measurement techniques, the average particle size of formulation F6 was found to be 112.9 nm, confirming its nanoscale dimensions.

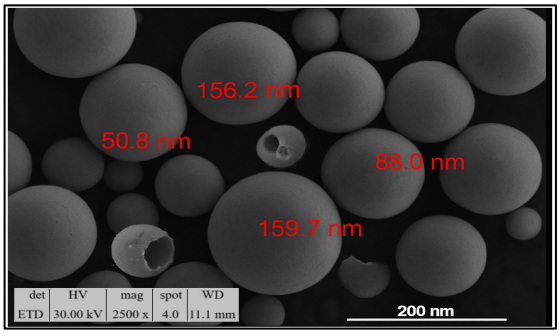

Figure 10. SEM image of F6 formulation

***In-vitro* Release Study of Nano-emulsion**

The *in-vitro* drug release of the *Artemisia Annua* L-loaded F6 nanoemulsion was assessed using a Franz diffusion cell (Figure 11). As detailed in Tables 12 and 13, F6 showed a maximum release 98.78±2.59%. The study was performed in phosphate buffer saline (PBS, pH 7.4) at 37°C with a 60-minute dialysis period. Drug release was measured using a UV-visible spectrophotometer. An initial burst release was observed, likely due to the small particle size offering a greater surface area and drug diffusion from the outer layer of the nanoemulsion.

Table 12. Formulation of F6

Sr. No.	Ingredients	Quantity
1	*Artemisia Annua* L	50 mg
2	Surfactant (Tween 80)	24%
3	Co-surfactant (PEG 400)	10%
4	Oil (Camelina sativa oil)	7%

Table 13. *In-vitro* release profile of Nano-emulsion

Sr. No.	Time (Hours)	Nano-emulsion (F6)
1	0	0
2	1	8.83±1.59
3	2	15.16±2.18
4	3	28.27±1.91
5	4	44.81±2.21
6	6	61.71±2.61
7	8	73.86±2.60
8	10	84.12±2.55
9	12	98.78±2.59

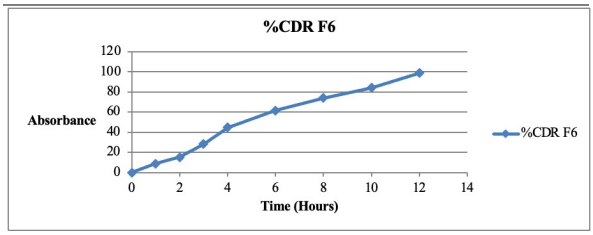

Figure 11. *In-vitro* drug release study of F6

Kinetics Study

The release kinetics of the F6 formulation are listed in Table 14 and shown in Figure 12. The in vitro results of the Artemisia annua L-loaded F6 nanoemulsion were evaluated using several kinetic models. The formulation demonstrated excellent linearity with zero-order kinetics (R^2 = 0.9735), indicating regulated drug release over 12 h. The Higuchi model (R^2 = 0.9448) demonstrated linearity, indicating diffusion-controlled release. The improved F6 formulation exhibited zero-order release kinetics and was most closely aligned with the Higuchi model.

Table 14. R^2 values of various Kinetic Models

Kinetic Model	R^2 Value (F6)
Zero order	0.9735
First order	0.7918
Higuchi	0.9448
Korsemeyer Peppas	0.8785

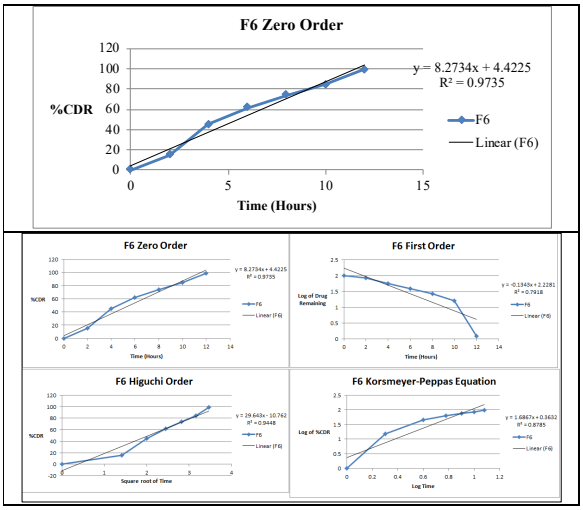

Figure 12. Kinetics of F6.

Stability Study

The optimized nanoemulsion (F6) was subjected to accelerated stability testing for three months under specified temperature and humidity conditions to evaluate its physicochemical robustness. The results presented in Table 15 indicate that the formulation maintained consistent characteristics throughout the study period, thereby confirming its stability.

The pH values showed only minor fluctuations, ranging from 7.02 ± 0.04 initially to 6.90 ± 0.08 at the end of three months. These small variations remained within acceptable limits and suggested the absence of chemical degradation or hydrolytic instability. Similarly, viscosity values remained relatively constant (78.45 ± 0.42 cps initially to 78.38 ± 0.44 cps at three months), indicating preservation of the internal structural integrity and rheological behavior of the nanoemulsion system.

The zeta potential showed minimal variation from –27.7 ± 0.01 mV to –26.96 ± 0.07 mV, demonstrating sustained electrostatic stabilization and absence of significant droplet aggregation. The maintenance of a sufficiently high negative surface charge throughout the storage confirms colloidal stability. Overall, the negligible changes observed in pH, viscosity, and zeta potential over the three-month period demonstrated that the optimized nanoemulsion (F6) possessed good physical stability under accelerated conditions, supporting its suitability for further pharmaceutical development.

Table 15. Stability analysis of the parameters of the improved formulation (F3)

Parameters	Initial Month	1st Month	2nd Month	3rd Month
pH	7.02±0.04	6.87±0.04	7.00±0.07	6.90±0.08
Viscosity (cps)	78.45±0.42	78.88±0.45	77.76±0.34	78.38±0.44
ZP (mV)	-27.7±0.01	-27.11±0.04	-27.55±0.06	-26.96±0.07

***In vivo* Antidiabetic Activity of Extract and Optimized Nanoemulsion**

Effect of AAE and AAN on Body Weight in Diabetic Rats

Repeated-measures mixed-model analysis demonstrated a substantial significant impact of group. ($p < 0.001$), day ($p < 0.001$), and a significant Group 21 Day interaction, indicating differential weight changes across the treatment groups. Post-hoc Tukey tests at Day 21 showed that the diabetic control group had significantly lower body weight than the normal controls (–69.9 g, $p < 0.001$). Treatment with metformin (25.8 g higher vs diabetic, $p < 0.001$), AAE 200 mg/kg (+55.6 g, $p < 0.001$), and AAN 200 mg/kg (+61.6 g, $p < 0.001$) significantly restored body weight compared with diabetic rats. On Day 21, AAN 200 mg/kg also differed significantly from AAE 200 mg/kg (+6.0 g, $p < 0.05$), suggesting superior efficacy of the nanoemulsion formulation (**Figure 13**).

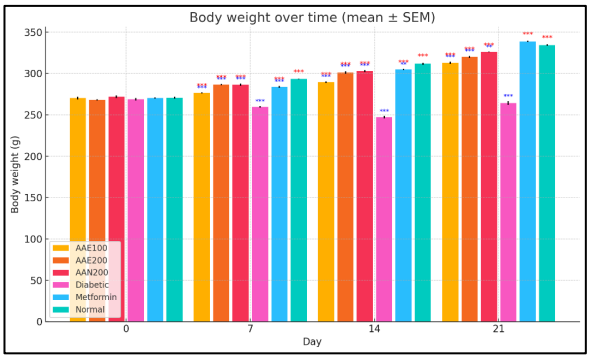

Figure 13. Impact of AAE and AAN on body weight in STZ–nicotinamide–induced diabetic rats over 21 days. Data are expressed as mean ± SEM (n = 6). Groups included Normal control, Diabetic control, Metformin (100 mg/kg), AAE (100 & 200 mg/kg), and AAN (200 mg/kg). One-way ANOVA with Tukey's post hoc test was used for statistical analysis. Red stars denote significance versus Diabetic control (*p < 0.05,

**p < 0.01, ***p < 0.001); blue stars denote significance versus Normal control.

Effect on Fasting Serum Glucose Levels

Mixed-model analysis confirmed the significant group, time, and interaction effects ($p < 0.001$). On Day 21, diabetic rats had markedly elevated glucose levels compared with normal controls (+165.4 mg/dL, $p < 0.001$). Metformin significantly reduced glucose levels relative to diabetic controls (–123.5 mg/dL, $p < 0.001$). AAE 200 mg/kg (–118.9 mg/dL, $p < 0.001$) and AAN 200 mg/kg (–126.1 mg/dL, $p < 0.001$) produced robust reductions in fasting glucose levels. AAN 200 mg/kg achieved glucose-lowering that was statistically indistinguishable from metformin (difference = +2.6 mg/dL, $p > 0.05$). AAE 100 mg/kg showed a partial reduction compared with diabetic controls (–105.2 mg/dL, $p < 0.001$), but remained higher than metformin and nanoemulsion treatments (**Figure 14**).

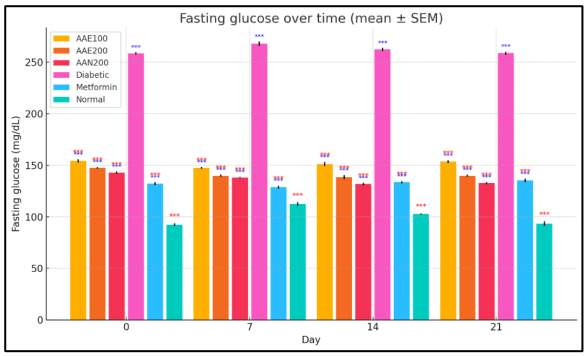

Figure 14. Impact of AAE and AAN on fasting blood glucose in diabetic rats over 21 days. Values are mean ± SEM (n = 6). One-way ANOVA with Tukey's post hoc test was applied; red stars denote significance versus Diabetic control, blue stars versus Normal control.

Effect on Biochemical and Oxidative Stress

Lipid profile (Day 21)

One-way ANOVA revealed significant group differences for all lipid parameters: TC ($F = 155.5$, $p < 0.001$), TG ($F = 220.8$, $p < 0.001$), HDL ($F = 65.6$, $p < 0.001$), VLDL ($F = 117.2$, $p < 0.001$), and LDL ($F = 133.2$, $p < 0.001$). Diabetic rats displayed pronounced dyslipidemia (↑TC, ↑TG, ↑VLDL, ↑LDL, ↓HDL) compared to normal controls. Treatment with metformin, AAE 200 mg/kg, and AAN 200 mg/kg significantly reduced TC (–51.9, –36.0, and –43.0 mg/dL vs diabetic, respectively; all $p < 0.001$) and TG (–67.0, –46.0, –55.0 mg/dL; all $p < 0.001$). HDL was significantly improved by AAE 200 and AAN 200 (+13.0 and +15.0 mg/dL vs diabetic, respectively; $p < 0.01$). AAN 200 produced numerically greater reductions in LDL (–40.6 mg/dL vs diabetic, $p < 0.001$) compared with AAE 200 (–30.6 mg/dL, $p < 0.001$) (**Figure 15**).

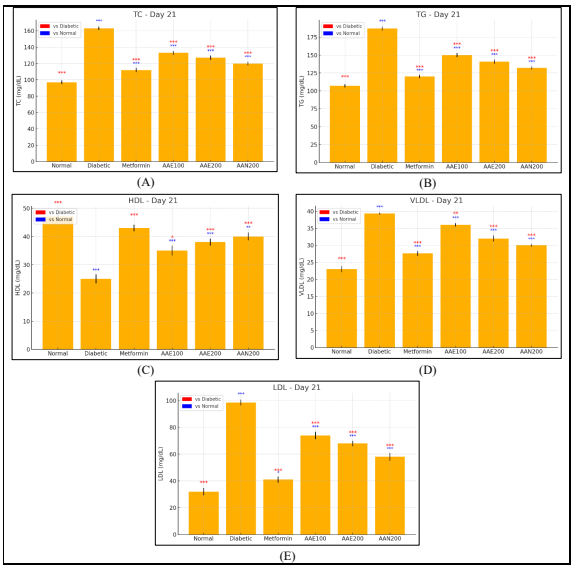

Figure 15. A) Total serum cholesterol levels (mg/dL); B) Serum triglyceride levels (mg/dL); C) Serum HDL cholesterol levels (mg/dL); D) Serum VLDL cholesterol levels (mg/dL); E) Serum LDL cholesterol levels (mg/dL) on Day 21. Values are shown as mean ± SEM (n = 6). Significance of stars: red indicates Diabetic, blue indicates Normal.

Oxidative stress and antioxidant markers (Day 21)

The ANOVA indicated significant group effects for all parameters: SOD ($F = 2.8$, $p = 0.035$), MDA ($F = 19.1$, $p < 0.001$), CAT ($F = 29.4$, $p < 0.001$), and GSH ($F = 4.0$, $p = 0.006$). Diabetic rats showed decreased antioxidant enzyme activities (SOD, CAT, and GSH) and elevated MDA levels compared to normal controls. Metformin significantly restored SOD (+3.5 U/mL vs diabetic, $p < 0.001$), CAT (+18.9 U/mg, $p < 0.001$), and GSH (+2.7 mg/dL, $p < 0.001$), while lowering MDA (–4.0 nmol/mL, $p < 0.001$). AAN 200 mg/kg produced significant improvements in all markers compared with diabetic controls (CAT +15.1 U/mg, $p < 0.001$; MDA –3.1 nmol/mL, $p < 0.001$), with effects approaching those of metformin. AAE at 200 mg/kg showed moderate but significant antioxidant restoration (**Figure 16**).

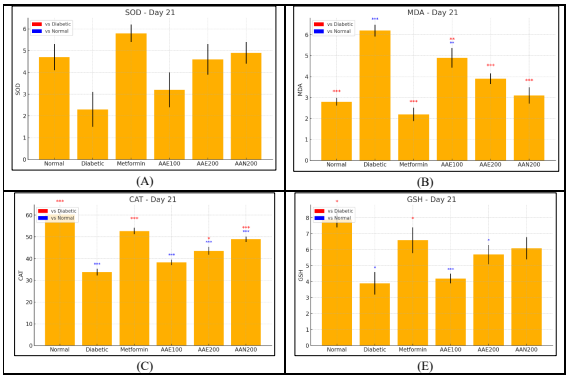

Figure 16. A) Superoxide dismutase (SOD) activity (U/mL); B) Malondialdehyde (MDA) concentration (nmol/mL); C) Catalase (CAT) activity (U/mg protein); D) Reduced glutathione (GSH) levels (mg/dL) on Day 21. Values represent mean ± SEM (n = 6). Significance: red = vs Diabetic, blue = vs Normal.

Liver function enzymes (Day 21)

Significant differences among the groups were observed for SGOT ($F \approx 100.5$, $p < 0.001$) and SGPT ($F \approx 597.6$, $p < 0.001$). Diabetic rats had elevated SGOT (+34.9 U/L vs normal, $p < 0.001$) and SGPT (+57.9 U/L, $p < 0.001$). Metformin, AAE 200, and AAN 200 significantly reduced both enzymes compared to diabetic controls (SGPT reductions: –46.2, –23.1, and –33.9 U/L, respectively; all $p < 0.001$). Among the treatments, AAN 200 achieved greater normalization of SGOT/SGPT than AAE 200 (**Figure 17**).

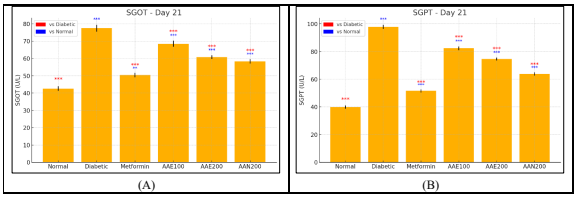

Figure 17. A) Serum glutamate oxaloacetate transaminase (SGOT) activity (U/L); B) Serum glutamate pyruvate transaminase (SGPT) activity (U/L) on Day 21. Values are shown as mean ± SEM (n = 6). Red stars indicate relevance in comparison to Diabetic, whereas blue stars indicate significance in comparison to Normal.

Conclusion

This study successfully developed and optimized an Artemisia annua L.-loaded nanoemulsion using a 2^3 factorial design to overcome the limitations of the crude extract. The optimized formulation (F6) exhibited nanoscale particle size (112.9 nm), high entrapment efficiency (89.2%), acceptable zeta potential (–27.7 mV), controlled drug release (98.78% over 12 h following Higuchi kinetics), and stability under accelerated conditions for three months. Biological evaluation demonstrated significant reduction in fasting blood glucose (–126.1 mg/dL), improvement in body weight, favorable modulation of lipid profile parameters, enhancement of antioxidant markers (SOD, CAT, GSH), reduction of MDA levels, and decreased elevated liver enzyme levels compared to the crude extract. These findings confirm that nanoemulsion-based delivery improves both the physicochemical characteristics and biological performance of Artemisia annua extracts. However, this study was limited to preclinical evaluations in an experimental animal model and short-term stability assessments. Long-term safety, pharmacokinetic profiling, and clinical validation in human subjects have not been performed. Future research should focus on extended stability studies, detailed bioavailability and pharmacokinetic investigations, dose-optimization studies, and large-scale clinical trials to validate the therapeutic efficacy and safety. Additionally, scaling-up strategies and regulatory evaluations should be explored to facilitate their translation into practical pharmaceutical applications. Overall, the optimized nanoemulsion represents a promising formulation strategy for enhancing plant-based therapeutic interventions in type 2 diabetes management.

Acknowledgements/Funding

The authors gratefully acknowledge Qassim University, represented by the Deanship of Graduate Studies and Scientific Research, for financial support for this research under the number QU-J-UG-2-2025-55637 during the academic year 1446 AH / 2025 CE.

Ethical Statement

All experimental procedures involving animals were conducted in strict accordance with the guidelines of the Committee for the Purpose of Control and Supervision of Experiments on Animals (CPCSEA), Government of India. The study protocol was reviewed and approved by the Institutional Animal Ethics Committee (IAEC) under the approval number 10/IAEC-II/SLSRPL/2025.

Credit authorship contribution statement

Writing – original draft, Visualization, Software, Project administration, Methodology, Investigation, Funding acquisition, formal analysis, data curation, conceptualization Mohd Masih Uzzaman Khan and Writing – original draft, Visualization, Software, Methodology, and Investigation by Faris Khalid AlForaiheedi.

Declaration of competing interest

The authors declare that they have no known competing financial interests or personal relationships that could have influenced the work reported in this study.

Data availability

No data was used for the research described in the article.

References

1. Naseri MW, Esmat HA, Bahee MD. Prevalence of hypertension in Type-2 diabetes mellitus. Ann Med Surg 2022; 78. doi: 10.1016/j.amsu.2022.103758
2. Yan Y, Wu T, Zhang M, Li C, Liu Q, Li F. Prevalence, awareness and control of type 2 diabetes mellitus and risk factors in Chinese elderly population. BMC Public Health 2022; 22. doi: 10.1186/s12889-022-13759-9
3. Hiasat DA, Salih MB, Abu Jaber AH, Abubaker OF, Qandeel YA, Saleem BA, Aburumman SI, Al-Sayyed ARH, Hussein TI, Hyassat D. The prevalence of diabetes distress among patients with type 2 diabetes in Jordan. J Taibah Univ Med Sci 2023; 18: 1237–43.
4. Tamboli AS, Tayade SD. In-Depth Investigation of Berberine and Tropane through Computational Screening as Possible DPP-IV inhibitors for the Treatment of T2DM. J Pharm Sci Comput Chem 2025; 1: 1–11.
5. Shastri MA, Gadhave R, Talath S, Wali AF, Hani U, Puri S, Rathod B, Khan SL. In silico Screening, Synthesis, and in vitro Enzyme Assay of Some 1,2,3-Oxadiazole-linked Tetrahydropyrimidine-5-carboxylate Derivatives as DPP-IV Inhibitors for Treatment of T2DM. Chem Methodol 2024; 8: 800–19.
6. Zinatloo-Ajabshir S, Mahmoudi-Moghaddam H, Amiri M, Akbari Javar H. A green route for the synthesis of sponge-like Pr6O11 nanoparticles and their application for the development of chlorambucil sensor. Meas J Int Meas Confed 2024; 235. doi: 10.1016/j.measurement.2024.114924
7. Zinatloo-Ajabshir S, Mahmoudi-Moghaddam H, Amiri M, Akbari Javar H. A green and simple procedure to synthesize dysprosium cerate plate-like nanostructures and their application in the electrochemical sensing of mesalazine. J Mater Sci Mater Electron 2024; 35. doi: 10.1007/s10854-024-12137-y
8. Zinatloo-Ajabshir Z, Zinatloo-Ajabshir S. Preparation and characterization of curcumin niosomal nanoparticles via a simple and eco-friendly route. J Nanostructures 2019; 9: 784–90.
9. Abboud HJ, Mahmoud ZH, Saadoun AM, Abdul Kareem EA, Mudhafar M, Lahhob QR, Mhaibes RM. MoS2 nanosheets-modified screen-printed electrode for the simultaneous detection of carmoisine and tartrazine. J Electrochem Sci Eng 2025; 15. doi: 10.5599/jese.2620
10. Ashaolu TJ. Nanoemulsions for health, food, and cosmetics: a review. Environ Chem Lett 2021; 19: 3381–95.
11. Souto EB, Cano A, Martins-Gomes C, Coutinho TE, Zielińska A, Silva AM. Microemulsions and Nanoemulsions in Skin Drug Delivery. Bioengineering 2022; 9. doi: 10.3390/bioengineering9040158
12. Aswathanarayan JB, Vittal RR. Nanoemulsions and Their Potential Applications in Food Industry. Front Sustain Food Syst 2019; 3. doi: 10.3389/fsufs.2019.00095
13. Wilson RJ, Li Y, Yang G, Zhao CX. Nanoemulsions for drug delivery. Particuology 2022; 64: 85–97.
14. Abate G, Zhang L, Pucci M, Morbini G, Sweeney E Mac, Maccarinelli G, Ribaudo G, Gianoncelli A, Uberti D, Memo M, Lucini L, Mastinu A. Phytochemical analysis and anti-inflammatory activity of different ethanolic phyto-extracts of artemisia annua l. Biomolecules 2021; 11. doi: 10.3390/biom11070975
15. Feng X, Cao S, Qiu F, Zhang B. Traditional application and modern pharmacological research of Artemisia annua L. Pharmacol Ther 2020; 216. doi: 10.1016/j.pharmthera.2020.107650
16. Mirbehbahani FS, Hejazi F, Najmoddin N, Asefnejad A. Artemisia annua L. as a promising medicinal plant for powerful wound healing applications. Prog Biomater 2020; 9: 139–51.
17. Ding F, Ma T, Hao M, Wang Q, Chen S, Wang D, Huang L, Zhang X, Jiang D. Mapping worldwide environmental suitability for artemisia annua L. Sustain 2020; 12. doi: 10.3390/su12041309
18. Al-Khayri JM, Sudheer WN, Lakshmaiah V V., Mukherjee E, Nizam A, Thiruvengadam M, Nagella P, Alessa FM, Al-Mssallem MQ, Rezk

AA, Shehata WF, Attimarad M. Biotechnological Approaches for Production of Artemisinin, an Anti-Malarial Drug from Artemisia annua L. Molecules 2022; 27. doi: 10.3390/molecules27093040

19. Babacan Ü, Cengiz MF, Bouali M, Tongur T, Mutlu SS, Gülmez E. Determination, solvent extraction, and purification of artemisinin from Artemisia annua L. J Appl Res Med Aromat Plants 2022; 28. doi: 10.1016/j.jarmap.2021.100363
20. Derda M, Hadaś E, Cholewiński M, Skrzypczak Ł, Grzondziel A, Wojtkowiak-Giera A. Artemisia annua L. as a plant with potential use in the treatment of acanthamoebiasis. Parasitol Res 2016; 115: 1635–9.
21. Jahangirian H, Lemraski EG, Webster TJ, Rafiee-Moghaddam R, Abdollahi Y. A review of drug delivery systems based on nanotechnology and green chemistry: Green nanomedicine. Int J Nanomedicine 2017; 12: 2957–78.
22. Kanwar R, Rathee J, Salunke DB, Mehta SK. Green nanotechnology-driven drug delivery assemblies. ACS Omega 2019; 4: 8804–15.
23. Bordean ME, Ungur RA, Toc DA, Borda IM, Marțiș GS, Pop CR, Filip M, Vlassa M, Nasui BA, Pop A, Cinteză D, Popa FL, Marian S, Szanto LG, Muste S. Antibacterial and Phytochemical Screening of Artemisia Species. Antioxidants 2023; 12. doi: 10.3390/antiox12030596
24. Abid KY, Abachi FT. Phytochemical Comparative Studies, Antioxidant and Antimicrobial of Artemisia and Star Anise. Pharmacogn J 2023; 15: 183–8.
25. Chinala KM, Chaithanya A, Sawrov M, Sahithi A, Achyuth C. Phytochemical and Antimicrobial Evaluation of Laurus nobilis Leaves Against Acne and Dandruff-Causing Microorganisms. J Pharm Sci Comput Chem 2025; 1: 50–7.
26. Khan SL, Bakshi V. LC-HRMS and In Silico Analysis of Ailanthus excelsa Metabolites Targeting EGFR Triple Mutation (L858R/T790M/C797S). Adv J Chem Sect A 2026; 9: 292–311.
27. Joshi M, Pathan I, Sahu A, Raza A, Sahu Y, Khatoon N. Computational Chemistry in Structure-Based Drug Design: Tools, Trends, and Transformations. J Pharm Sci Comput Chem 2025; 1: 246–66.
28. Hani U, Al-Qahtani EH, Albeeshi FF, Alshahrani SS. Exploring the Landscape of Drug-Target Interactions: Molecular Mechanisms, Analytical Approaches, and Case Studies. J Pharm Sci Comput Chem 2025; 1: 12–25.
29. Wang X, Tian C, Sun F, Wu S, Jiang Q, Ji K, Li R. Synthesis of a novel Guar gum-bentonite composite for effective removal of Pb(II) species from wastewater: Studies on isotherms, kinetics,thermodynamic and adsorption mechanisms. Desalin Water Treat 2024; 319: 100424.
30. Nafisi S, Saboury AA, Keramat N, Neault JF, Tajmir-Riahi HA. Stability and structural features of DNA intercalation with ethidium bromide, acridine orange and methylene blue. J Mol Struct 2007; 827: 35–43.
31. Shah Bukhary SKH, Choudhary FK, Iqbal DN, Ali Z, Sadiqa A, Latif S, Al-Ahmary KM, Basheer S, Ali I, Ahmed M. Development and characterization of a biodegradable film based on guar gum-gelatin@sodium alginate for a sustainable environment. RSC Adv 2024; 14: 19349–61.
32. Daud H, Ghani A, Iqbal DN, Ahmad N, Nazir S, Muhammad MJ, Hussain EA, Nazir A, Iqbal M. Preparation and characterization of guar gum based biopolymeric hydrogels for controlled release of antihypertensive drug. Arab J Chem 2021; 14. doi: 10.1016/j.arabjc.2021.103111
33. Jadhav SS, Dighe PR, Kumbhare MR. Synthesis, In Vitro Evaluation, and Molecular Docking Studies of Novel Pyrazoline Derivatives as Promising Bioactive Molecules. J Pharm Sci Comput Chem 2025
34. Osanloo M, Alipanah H, Hashempour M, Zarenezhad E, Motazedian B, Zahedifard Z, Ghasemian A. The antimicrobial and antibiofilm potential of Citrus aurantium and Artemisia annua essential oils nanoemulsions against standard and multidrug-resistant nosocomial pathogens. Arch Razi Inst 2024. doi: 10.32592/ARI.2025.80.4.927
35. Thuraisingam S, Salim N, Azmi IDM, Kassim NK, Basri H. Development of Nanoemulsion containing Centella Asiatica Crude Extract as a Promising Drug Delivery System for Epilepsy Treatment. Biointerface Res Appl Chem 2023; 13. doi: 10.33263/BRIAC131.017

36. Al-Hakim NA, Fidrianny I, Anggadiredja K, Mauludin R. Effect of Banana (Musa sp.) Peels Extract in Nanoemulsion Dosage Forms for the Improvement of Memory: In Vitro & In Vivo Studies . Pharm Nanotechnol 2022; 10: 299–309.